Multi-physics numerical simulation study on thermo-sensitive gel delivery for a local post-tumor surgery treatment

González-Garcinuño, Álvaro; Tabernero, Antonio; Blanco-López, Marcos; Martín del Valle, Eva; Kenjeres, Sasa

DOI
10.1016/j.ejps.2024.106917

Publication date
2024

Document Version
Final published version

Published in
European Journal of Pharmaceutical Sciences

European Journal of Pharmaceutical Sciences 203 (2024) 106917

Contents lists available at ScienceDirect

European Journal of Pharmaceutical Sciences

journal homepage: www.elsevier.com/locate/ejps

Multi-physics numerical simulation study on thermo-sensitive gel delivery for a local post-tumor surgery treatment

Álvaro González-Garcinuño [a,b,*], Antonio Tabernero [a,b], Marcos Blanco-López [a], Eva Martín del Valle [a,b], Sasa Kenjeres [c,*]

[a] Department of Chemical Engineering. University of Salamanca. Plaza Los Caídos s/n, 37008 Salamanca, Spain
[b] Institute for Biomedical Research in Salamanca (IBSAL), Paseo de San Vicente 87, 37007, Salamanca, Spain
[c] Department of Chemical Engineering, Faculty of Applied Sciences, Delft University of Technology, Delft, Van der Maasweg 9, 2629 HZ Delft, the Netherlands

ARTICLE INFO

Keywords:
Thermo-responsive hydrogel
Multi-physics simulations
Injection
Level set method
Gelation

ABSTRACT

Numerous studies in the literature have proposed the use of thermo-responsive hydrogels for filling cavities after tumor resection. However, optimizing the injection process is challenging due to the complex interplay of various multi-physics phenomena, such as the coupling of flow and heat transfer, multi-phase interactions, and phase-change dynamics. Therefore, gaining a fundamental understanding of these processes is crucial. In this study, we introduce a thermo-sensitive hydrogel formulated with poloxamer 407 and Gellan gum as a promising filling agent, offering an ideal phase-transition temperature along with suitable elastic and viscous modulus properties.

We performed multi-physics simulations to predict the flow and temperature distributions during hydrogel injection. The results suggested that the hydrogel should be kept at 4 °C and injected within 90 s to avoid reaching the transition temperature. Cavity filling simulations indicated a symmetric distribution of the hydrogel, with minimal influence from the syringe's position.

The temperature gradient at the cavity edge delays gelation during injection, which is essential to guarantee its administration as a liquid. The hydrogel's viscosity follows a sigmoidal function relative to temperature, taking five minutes to reach its maximum value. In summary, the multi-physics simulations carried out in this study confirm the potential of thermo-responsive hydrogels for use in post-tumor surgery treatment and define the conditions for a proper administration. Furthermore, the proposed model can be widely applied to other thermo-responsive hydrogels or under different conditions.

1. Introduction

Cancer presents a global health challenge that requires innovative approaches to improve the effectiveness of therapeutic interventions while reducing systemic side effects. The traditional systemic administration of anticancer agents often results in the widespread distribution of drugs throughout the body, leading to dose-limiting toxicity and reduced therapeutic efficacy. Among the emerging strategies, hydrogels are becoming increasingly significant as they can fill cavities post-tumor resection and their properties can be adjusted by altering factors such as polymer type, crosslinking degree, transition temperature, etc.

Recent studies have demonstrated the use of hydrogels for treating various types of cancer, including ovarian (Xu et al., 2018) and lung (Lv et al., 2020). Additionally, another hydrogel, OncoGel™ developed several years ago for glioma treatment (Elstad and Fowers, 2009), is currently undergoing clinical trials.

The application of these hydrogels for breast cancer treatment is considered particularly promising due to the specific characteristics of this cancer type: ease of administration, clear diagnostic images prior to administration, and the absence of surrounding tissues. Furthermore, these hydrogels can help in breast reconstruction (Yang et al., 2021). The use of hydrogels as a post-resection therapy for breast tumors has been extensively reviewed (Zhang et al., 2022).

In recent years, significant efforts have been dedicated to harnessing the distinctive properties of thermo-sensitive hydrogels. These "intelligent biomaterials" can undergo reversible phase transitions in response to external stimuli, such as temperature changes, making them a promising option for precise and localized drug delivery in cancer therapy. In this regard, thermo-sensitive hydrogels stand out as an advanced solution to tackle these challenges by providing a platform for controlled drug release at the tumor site (Lacroce and Rossi, 2022;

* Corresponding authors.
E-mail addresses: alvaro_gonzalez@usal.es (Á. González-Garcinuño), s.kenjeres@tudelft.nl (S. Kenjeres).

https://doi.org/10.1016/j.ejps.2024.106917
Received 2 July 2024; Received in revised form 5 September 2024; Accepted 27 September 2024
Available online 28 September 2024

Nomenclature

ρ	density, kg/m^3
u	fluid velocity, m s^{-1}
τ	Shear stress, Pa
I	identity tensor
g	gravity force, m s^{-12}
F	extra forces, N
T	temperature, K
F_{st}	stokes force, N
σ	surface tension value, N/m
k_i	curvature, dimensionless
n_{int}	unit normal to the interface, dimensionless
δ	Dirac delta function concentrated to the interface, m
φ	level set function, dimensionless
Cp	Specific heat at constant pressure, J/kg•K
q	conductive heat flux vector, W/m^2
q_0	heat flux at the boundaries, W/m^2
Q	heat supplied to the system, W/m^3
k	thermal conductivity, W/m•K
Tout	operation suite temperature, K
Tw	temperature at the wall, K
h	heat transfer coefficient, W/m^2•K
γ	amount of reinitialization or stabilization of the level set function, m s^{-1}
εls	thickness of the interphase region, m
I(φ)	Heaviside function for level set function, dimensionless
μ	viscosity, Pa•s
t	time, s

Mohammadi et al., 2022).

One of the most studied polymers for this purpose is Poloxamer 407, also known as Pluronic F-127. This thermosensitive polymer not only inhibits breast cancer resistance protein (BCRP) but has also been approved by the FDA (Shriky et al., 2020; Ul Khaliq et al., 2023). Hydrogels formed with this polymer maintain a liquid state at low temperatures and transition into a non-flowing gel at temperatures close to the physiological range (37ºC). This characteristic is crucial for accurate administration and stable drug release in the cavity post-surgery (De Dios-Perez et al., 2023).

The temperature for the sol-gel transition is influenced by the poloxamer concentration in the hydrogel. Lower concentrations, starting at 15% w/v, are associated with higher transition temperatures, making them easier to administer at room temperature (Kushan and Senses, 2021). However, a high poloxamer concentration is necessary to ensure proper behavior in vivo. Jons et al. (2022) demonstrated a significant correlation between the storage modulus (G') and the hydrogel's persistence in tissue, indicating that hydrogels with G' values exceeding 100 Pa can persist for over 30 days in mice. Additionally, Yang et al. (2021) suggested that hydrogels used for cavity filling after breast tumor resection should have a G' value around 104 Pa, achievable only with PF-127 concentrations exceeding 20 %.

Moreover, the rheological properties of hydrogels can be altered by incorporating other polysaccharides such as chitosan, sodium alginate, gellan gum, or carrageenan (Lupu et al., 2023). Among these, gellan gum (GG) shows promise in regulating thermogelation as even a small concentration of it significantly impacts the gelation temperature and hydrogel viscosity (Dewan et al., 2017). In a previous study, various formulations of PF-127 were prepared to investigate farnesol drug release. The findings revealed that adding 0.5% w/v of GG to a 20% w/v PF-127 solution extended the degradation time of the formulation (due to the formation of a new polymer network with the addition of GG) and altered the drug release profile (De Dios-Pérez et al., 2023). Therefore, this study will combine PF-127 and GG in the designed hydrogels for these reasons.

According to the latest review on hydrogels from poloxamers by Marques et al. (2023), numerous studies have focused on the rheological behavior and mechanical strength of these hydrogels. However, there is limited literature on their injectability, despite it being a critical parameter. Some papers have computationally investigated hydrogel injection for treating myocardial diseases. For instance, Wang et al. (2018) and Fan et al. (2019) examined the stress in heart cavities post-hydrogel injection following myocardial infarction. Similarly, Curley et al. (2017) compared various types of needles and polymers for myocardial injection.

In addition to cardiac applications, other researchers have explored the use of hydrogels for various purposes. For instance, Phogat et al. (2023) examined the injectability of hydrogels for bone tissue rehabilitation from a rheological perspective, focusing on factors such as the required pressure, interactions between components, and cohesion. Similarly, Rossi et al. (2019) conducted injectability studies using uniaxial tensile testing with various syringe and needle sizes, although they did not account for the temperature effect in their simulations.

In the case of PF-127, only four studies, to the best of our knowledge, have studied injectability to varying degrees. Soni and Yadav (2014) demonstrated the ability to inject hydrogels at temperatures below 17 °C, although the administration temperature always exceeds this threshold. Additionally, Braet et al. (2021) explored the intraperitoneal administration of PF-127 nanoparticles through nebulization at high pressures for cancer treatment. Furthermore, Emerson et al. (2022) developed a model to predict the size and shape of hydrogels containing cells and other polysaccharides such as alginate or agarose.

Finally, the only study regarding PF-127 administration via syringe is the one conducted by Yu and Chen (2021). In their research, the authors performed simulations on the coaxial extrusion of PF-127 hydrogel to investigate viscosity variations. However, they did not account for property changes due to temperature (crucial for thermosensitive polymers) and solely focused on analyzing the mixture, neglecting the process of deposition in a cavity.

Due to the lack of research justification, there is a strong need to study the administration of thermosensitive hydrogels during surgery to facilitate the transfer of this technology to real clinical practice (Mandal et al., 2020; Clegg et al., 2024). These hydrogels are highly temperature-sensitive, and it is crucial that the sol-gel transition does not occur before the injection is completed. Additionally, ensuring correct deposition in the tumor cavity is essential for effective drug release, as these hydrogels can be loaded with chemotherapeutic agents to prevent cancer recurrence.

Therefore, the main objective of this work is to provide a computational approach, based on experimental data, to the optimal method for thermosensitive hydrogel injection and cavity filling. The proposed model will consider the viscosity-temperature dependency. To achieve this objective, real tumor cavity geometries obtained from MRI scans of patients will be used, along with experimental data on hydrogel formulations and their sol-gel transition characteristics. The study will generate the volume of fluid profiles (VOF) for cavity filling, along with temperature and viscosity profiles, to elucidate the process and provide a precise framework for translating these strategies into clinical practice. To validate the model, the PF-127 with the GG formulation described earlier was chosen for performing various simulations.

2. Materials and methods

2.1. Thermosensitive hydrogel preparation and characterization

The initial PF-127 solutions (20 % and 30% w/v) were prepared at 4 °C in distilled water, as indicated in De Dios-Pérez et al. (2023). To begin, the necessary amount of GG was dissolved in distilled water that had been previously heated to 80 °C. The solution was maintained at 80 °C and stirred for 1 hour to achieve a uniform bulk sample. Subsequently, the GG solution was allowed to cool slowly at room temperature. The cooled GG solution was then transferred to a cold chamber at 4 °C. Once the solution reached this temperature, the required amount of PF-127 was gradually added under stirring conditions. Finally, the hydrogel was left to stir overnight. In order to guarantee the sterility of the hydrogel for biomedical applications, the preparation should be carried out in a clean room, and all materials used must be previously sterilized by autoclaving and UV light exposure.

The PF-127 solutions underwent rheological characterization using an AR 1500 Rheometer (TA Instruments, Newark, DE) equipped with an aluminum plate of 40 mm and a 1 mm gap. An oscillation procedure was applied, involving a temperature sweep from 10 °C to 37 °C (with a temperature increase of 1 °C/min) at a frequency of 10 Hz and a strain percentage of 0.2 %. Under these conditions, the sample exhibited viscoelastic behavior (De Dios-Pérez et al., 2023). This procedure yielded the values of the storage (G') and loss (G'') moduli and their temperature-dependent variations. Additionally, steady-state analysis (at a shear rate of 50 s^{-1}) was conducted to investigate how temperature variations (from 10 °C to 37 °C) affected the viscosity of the different formulations.

2.2. Model geometry and meshing

Two different geometries were created using the geometry interface of COMSOL Multiphysics 6.1 for each step of the simulation. Firstly, dimensions for modeling the syringe and the needle were obtained from a catalog. The syringe was chosen with a volume of 5 mL, and a 23 Gauge needle was selected. This implies that the inner diameter of the syringe is 1.27 cm, and the inner diameter of the needle is 0.34 mm. PVC (polyvinyl chloride) was chosen as the material for the syringe walls, while stainless steel was selected for the needle walls.

Secondly, the geometry of the tumor cavity was constructed based on typical shapes and volumes found in breast tissue after tumor resection. The simulated cavity has a total volume of 12,818 mm^3 and is considered as an ellipsoid with the following dimensions: semi-axis a (15 mm), semi-axis b (17 mm), and semi-axis c (12 mm). These values were determined by isolating the tumor geometry from a dataset of MRI images of real patients (Saha et al., 2018). The resection cavity is open at the top border to simulate the opening or scar, with a diameter of 2 mm. At the top, the needle serves as the inlet (marked in blue) and has the same dimensions as described above. Both geometries are depicted in Fig. 1, A and B, showcasing 3D images and cross-sections of each.

The final meshes were constructed using tetrahedrons. The syringe's mesh consists of 1.93 million elements, with an average quality of 0.919 and the largest element size being 0.037 mm. The cavity's mesh comprises 97.3 thousand elements, with an average quality of 0.662 and the largest element size of 2.1 mm. Quality plots of both meshes can be found in Supplementary Material S1.

2.3. Mathematical modelling: governing equations and boundary conditions

To mimic the injection of the thermo-responsive hydrogel into the tumour post-resection cavity, one needs to consider the following physical transport phenomena: (i) in the simulation of the syringe and needle, a fluid flow is coupled with conjugate heat transfer, (ii) in the cavity filling simulations, these equations are extended with the multiphase level-set method to capture the hydrogel/air interface. Based on these considerations, this section is divided into four subsections, each focusing on a specific phenomenon studied.

2.3.1. Mass and momentum transport in laminar flow regime

The flow of hydrogel in the syringe and during the cavity filling can be described by equations for conservation of mass and momentum, which can be written as:

$$\rho\nabla\cdot\vec{u} = 0 \tag{1}$$

$$\rho\frac{\partial\vec{u}}{\partial t} + \rho(\vec{u}\cdot\nabla)\vec{u} = \nabla\cdot(-p\bar{I}+\bar{\tau}) + \rho\vec{g} + \vec{F} \tag{2}$$

where the shear stress is calculated as:

$$\bar{\tau} = \mu\left(\nabla\vec{u} + \nabla\vec{u}^{T}\right) \tag{3}$$

In both cases, gravity can not be considered negligible because the administration process takes advantage of gravity. For multi-phase simulations of the cavity filling, the surface tension force needs to be considered too:

$$\vec{F}_{st} = \sigma k_i \delta\,\vec{n}_{\text{int}} \tag{4}$$

where (σ) is the surface tension, (k_i) is the interface curvature, (n_{int}) is the unit vector normal to the interface, and (δ) is the Dirac's delta function concentrated at the interface. These are calculated as:

$$\vec{n}_{\text{int}} = \frac{\nabla\varphi}{|\nabla\varphi|}, k_i = \nabla\cdot\left(\frac{\nabla\varphi}{|\nabla\varphi|}\right), \delta = 6|\nabla\varphi||\varphi(1+\varphi)| \tag{5}$$

Here, (φ) represents the level-set function that will be explained in more detail in the following subsection.

The boundary conditions for fluid flow simulation in the syringe include: a no-slip condition at the wall, an outlet pressure equal to zero, and the inlet pressure simulated as a step function (with a duration of

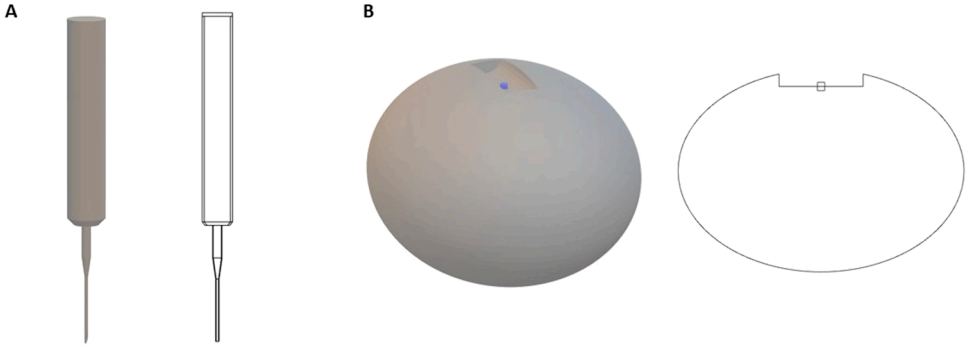

Fig. 1. A: Geometry of syringe and needle. B: Geometry used for simulating cavity filling simulations.

four seconds, changing the pressure at the inlet from 0 to 50 kPa). The calculation for the pressure condition was derived from data reported in the literature regarding the force applied to the plunger (Krisdiyanto et al., 2023) and can be automatized by using a pump.

The boundary conditions for fluid flow simulation in the cavity include a no-slip condition at the wall, a pressure of zero at the opening, and an inlet velocity equal to the one calculated at the outlet of the needle simulations.

2.3.2. Conjugate heat transfer

The heat transfer is modelled by using the following transport equation:

$$\rho c_p \frac{\partial T}{\partial t} + \rho c_p \vec{u} \cdot \nabla T + \nabla \cdot \vec{q} = Q \tag{6}$$

where the heat flux is calculated as:

$$\vec{q} = -k \nabla T \tag{7}$$

Note that the heat transfer model includes the calculation of temperature in both the fluid domain and surrounding walls (which are made from PVC or stainless steel). We considered two initial conditions during the injection step: (i) syringe, needle, and fluid are all kept at 4ºC before administration, and (ii) fluid is kept at 4ºC, whereas the syringe and needle are both kept at room temperature of 20ºC. For both scenarios, the convective heat transfer with the surrounding environment (air at 20ºC) is included, which is implemented through the following boundary condition:

$$q_0 = h(T_{air} - T_W) \tag{8}$$

During the filling process, the cavity wall temperature is fixed at 37ºC to mimic the physiological temperature of human tissue, while the temperature along the opening/scar is estimated using the aforementioned convective boundary condition. The specific heat under constant pressure (c_p) is assumed to be constant for both simulations.

2.3.3. The multi-phase simulation of the cavity filling

The multi-phase modeling of cavity filling is conducted using the level-set method of Osher and Sethian (1988). The hydrogel is injected into the cavity at a constant velocity determined from the previous simulation of fluid flow in the syringe. The volume of hydrogel injected in its liquid state displaces the air within the cavity resulting from tumor resection. The level-set function (φ) is defined to have a value of one in the air and a value of zero in the hydrogel. The time and spatial evolution of the hydrogel/air interface is calculated using the following transport equation:

$$\frac{\partial \varphi}{\partial t} + \vec{u} \cdot \nabla \varphi = \gamma \nabla \cdot \left[\varepsilon_{ls} \nabla \varphi - \varphi(1-\varphi) \frac{\nabla \varphi}{|\nabla \varphi|} \right] \tag{9}$$

Terms on the right-hand side are essential for numerical stability. To ensure the numerical stability and convergence of the multi-phase simulations, both (γ) and (ε_{ls}) should be fixed at the beginning of the simulations, as suggested by Yue et al. (2004). The first parameter (γ) represents the amount of the reinitialization or stabilization of the level set function (φ). Its value corresponds to the maximum velocity modulus in the entire domain. The second parameter (ε_{ls}) determines the thickness of the interface and should be set equal to the largest mesh element in the domain.

The level-set function (φ) takes the following forms of Heaviside function:

$$I(\varphi) = \begin{cases} 0, & if \quad \varphi < -\delta \cdot \Delta \\ \frac{1}{2}\left[1 + \varphi + \frac{1}{\pi}\sin\left(\frac{\pi \cdot \varphi}{\delta \cdot \Delta}\right)\right], & if |\varphi| \le \delta \cdot \Delta \\ 1, & if \quad \varphi > \delta \cdot \Delta \end{cases} \tag{10}$$

where (Δ) is the characteristic numerical mesh length scale, and (δ) is the previously defined Dirac delta function (see Eq. (5)). The cavity is assumed to be filled with air at the start of simulations. The velocity and temperature fields are calculated by solving conservation of mass, momentum and energy, but now for both phases (air-fluid as 1 and hydrogel-fluid as 2). Consequently, the physical properties (density, dynamic viscosity, thermal conductivity) are depending on the level set function (φ) and evaluated as:

$$\rho = \rho_1 + (\rho_2 - \rho_1)\varphi, \quad \mu = \mu_1 + (\mu_2 - \mu_1)\varphi, \quad k = k_1 + (k_2 - k_1)\varphi \tag{11}$$

The boundary conditions for the level set method are identical to those used in fluid flow and heat transfer described in Sections 2.3.1 and 2.3.2, respectively.

2.4. The sol-gel transition kinetics

The sol-gel transition is dependent on both temperature and the time at which the transition temperature is reached. This kinetic transition is generally considered quasi-instantaneous, although some studies have only approached it in a preliminary manner. According to Witika et al. (2021), the time for the sol-gel transition ranges from 5 to 7 min, depending on the PF-127 concentration (20–25 % wt) at 37ºC. Additionally, Petkova-Olsson et al. (2018) suggested that the evolution of viscosity should follow a sigmoidal curve, in accordance with the profiles obtained by Dynamic Wave Spectroscopy.

Based on the previous information, a simplified equation is proposed to define the dynamic viscosity behavior of thermosensitive hydrogels over time once the transition temperature is reached. The equation can be expressed as follows:

$$\mu(t) = 0.52 + \frac{9.1}{1 + \exp\left[-\frac{(t-150)}{30}\right]} \tag{12}$$

where the dynamic viscosity (μ) is in Pa•s, while time (t) is in seconds. This curve has an upper limit of 9.6 Pa•s and a lower limit of 0.58 Pa•s, which is consistent with the experimental results (see Section 3.1 and Supplementary material S2 for the results from the steady-state flow analysis). Additionally, the transition from the lower to the upper limit of this curve occurs within a time frame of five minutes, as indicated by Witika et al. (2021).

2.5. Parameters used for simulations

All simulation parameters, along with their corresponding reference sources, are given in Table 1. The table is divided into two sections, distinguished by the specific steps under investigation, namely syringe injection and cavity filling, respectively. It is important to note that certain values recorded in the first step are essential for the calculation of the second step. The model is also flexible and could be used for simulating other cases if the material or hydrogel properties change.

3. Results and discussion

The structure of this section is as follows: firstly, rheological measurements of the prepared hydrogels are presented to utilize this data for the multi-physics simulation. Subsequently, the results for syringe injection are discussed, followed by the results for tumor cavity filling.

3.1. Experimental determination of thermosensitive hydrogels properties and response to temperature

Fig. 2 shows the variation of G' (left axis) and G'' (right axis) with temperature until it reaches its maximum value. Additionally, G' exceeds 14 kPa for a 30% w/v formulation, while a value below 8 kPa was obtained with the 20% w/v solution. Fig. 2b depicts the variation of

Table 1
Parameters used for simulations.

Step	Parameter	Value	Units	*Reference*
Syringe injection	Plunger Pressure applied	50	kPa	Krisdiyanto et al., 2023
	Time for injection	14	s	Calculated from flow rate and syringe volume
	Initial temperature	4	ºC	Fridge temperature
	Operating suites temperature	20	ºC	Ellis, 1963
	Hydrogel density	1000	kg/m^3	Bui et al., 2021
	PVC density	1350	kg/m^3	
	Stainless steel density	8000	kg/m^3	
	Hydrogel viscosity (under 18ºC)	0.58	Pa•s	Experimental (this study)
	PVC thermal conductivity	0.19	W/(m•K)	Kok et al., 2008
	Stainless steel thermal conductivity	15	W/(m•K)	Meckky, 2020
	Hydrogel thermal conductivity	0.54	W/(m•K)	Milocco et al., 2020
	Air heat transfer coefficient (convection, free)	30	W/(m^2•K)	Xanthopoulos et al., 2012
	Hydrogel Specific Heat capacity	5000	J/(kg•K)	Milocco et al., 2020
	PVC Specific Heat capacity	880	J/(kg•K)	Kok et al., 2008
	Stainless steel Specific Heat capacity	477	J/(kg•K)	Meckky, 2020
Tumour Cavity filling	Surface tension of the hydrogel	0.036	N/m	Desai et al., 2001
	Air density	1.02	kg/m^3	
	Air viscosity	1.8•10^{-5}	Pa•s	
	Air conductivity	0.027	W/(m•K)	

viscosity in the formulation with temperature until reaching the maximum viscosity value. It is evident that the temperature transition for the formulation containing 30% w/v of PF-127 occurred at approximately 18 °C, while a transition temperature of around 27 °C was observed for the formulation with 20% w/v of PF-127. In this scenario, it is crucial to choose the formulation with 30% w/v as the G' value is suitable for filling the tumor cavity, as highlighted by Chenite et al. (2001).

3.2. Hydrogel injection studies

The injection was modeled as a step function lasting 14 s with a 50 kPa pressure at the top of the syringe, as indicated in Section 2.3.1. The velocity contours before and during injection are illustrated in Fig. 3a, while Fig. 3b represents the velocity contours during injection on a logarithmic scale to better highlight the differences.

It can be seen that the velocity field within the syringe exhibits a wide range of values. The fluid velocity reaches 4 m s^{-1} at the needle outlet, while within the middle section of the syringe, it remains below 0.1 m s^{-1}. Consequently, the syringe demonstrates a maximum flow rate of approximately 20 mL/min, consistent with the reported flow rates for the specific needle considered (Talu et al., 2008). Thus, the entire administration process of the hydrogel within the syringe takes around 14 s.

However, due to the thermosensitive characteristics of the hydrogel and the administration process taking place at 20ºC (operating suite temperature), the hydrogel may undergo the sol-gel transition, leading to a viscosity increase. This rise in viscosity could present challenges during the injection into the cavity. To evaluate the time constraints before reaching the transition temperature, two separate simulations were carried out to determine the maximum time available for administration.

Fig. 4 shows the time evolution of temperature three distinct locations within the device (needle outlet, hub, and in the middle of the barrel) under two different initial conditions: the hydrogel is stored in a fridge (4ºC) while the syringe and needle are at room temperature, or alternatively, the syringe, needle, and hydrogel are all kept at fridge temperature (4 °C).

In Fig. 4a, it is shown that if the initial conditions are 4ºC for all materials, it takes approximately 90 s to reach the transition temperature (18ºC) for the fluid in the needle outlet. However, this temperature is not reached in the fluid located in the hub or in the middle of the barrel. This discrepancy is attributed to the inner diameter of each part and the two orders of magnitude difference in thermal conductivity between stainless steel and PVC. Conversely, when the syringe and needle are maintained at 20ºC, similar profiles are observed for points one and two (Fig. 4b), with a significant difference observed at point three (green one).

At this juncture, the fluid exhibits a considerable increase in temperature during the initial seconds due to heat transfer from the plunger, eventually reaching a quasi-steady-state around 10ºC. These graphs are complemented by those presented in Fig. 5, where the temperature plots for the entire geometry for both cases can be observed.

Based on the results from Fig. 5, and considering the transition

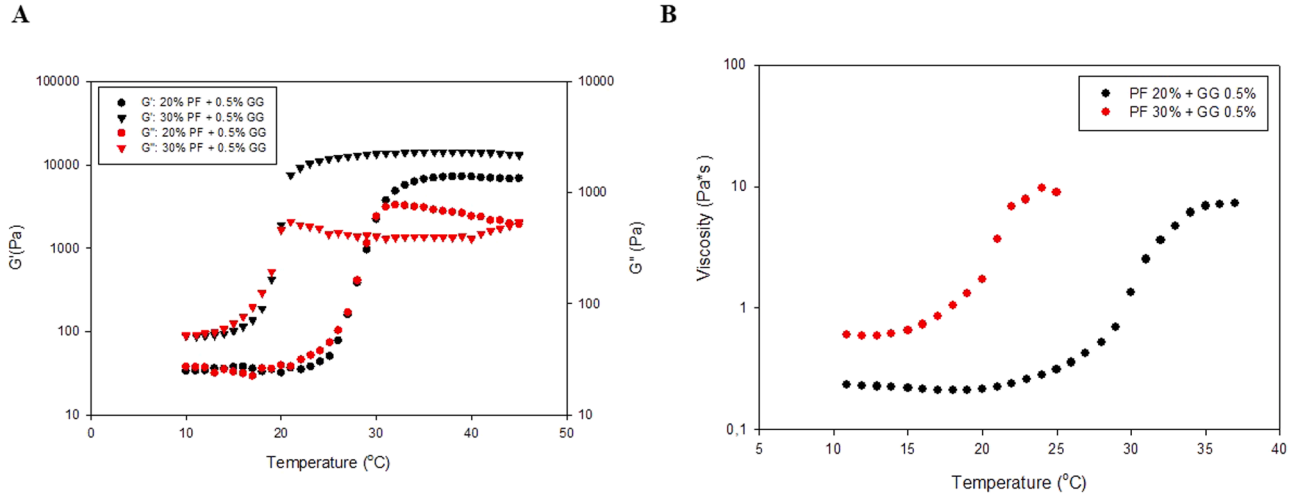

Fig. 2. Evolution of the G' and G'' (A) and viscosity (B) with temperature for two different PF-127 concentrations (20 % and 30% w/v) with 0.5% w/v GG.

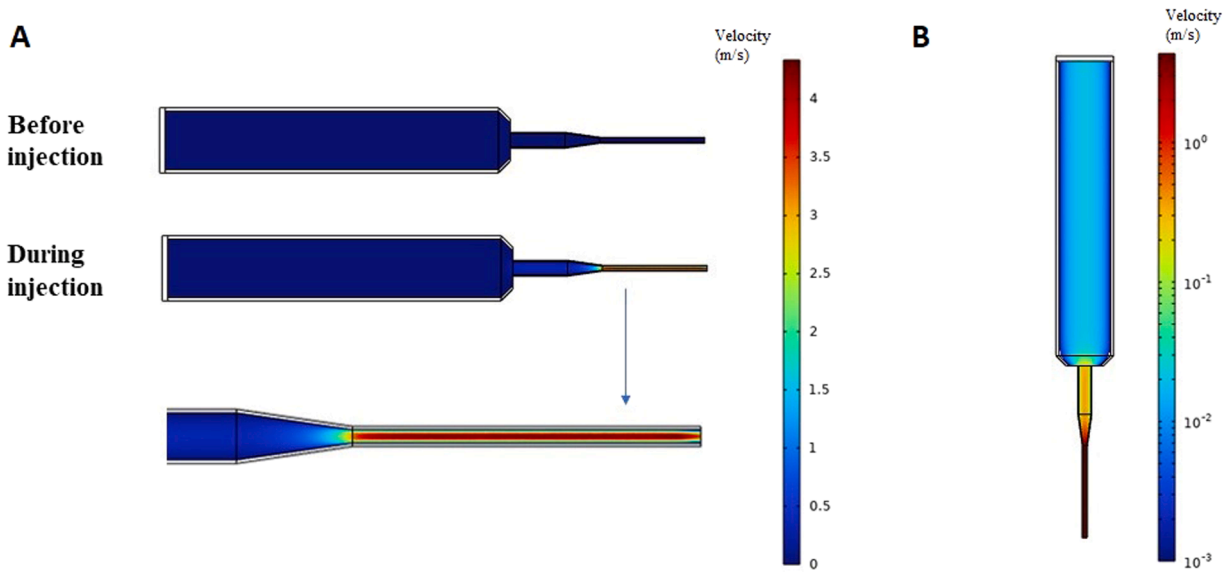

Fig. 3. Velocity contours before and during hydrogel injection (A); Velocity contours during hydrogel injection in logarithmic scale (B).

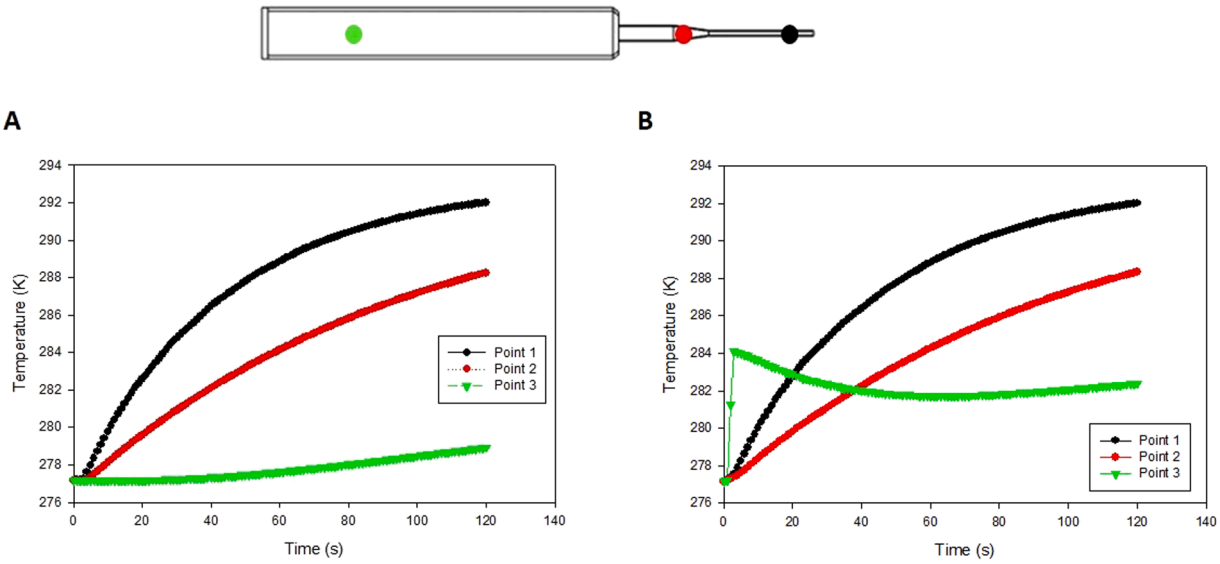

Fig. 4. Time evolution of the hydrogel temperature at three different locations of the device depending on the syringe and needle storage: A: at 4ºC, B: at 20ºC. Colour legend: Needle outlet (black), hub (red), middle of the barrel (green).

temperature is 18ºC, the syringe and needle can be kept at room temperature. However, it is crucial that the administration process takes <90 s from the moment the hydrogel solution is removed from the fridge. This value is estimated for a thermostated surgical theatre (20 °C) and variations in this temperature can reduce or increase the maximum time available for administration. This time constraint is a critical factor to consider for any potential clinical application of the tested hydrogel.

3.3. Cavity filling studies

During the surgery, the tumor mass is resected, leaving a space initially filled with air that is in contact with the environment through the aperture. Subsequently, this space is filled with the hydrogel solution. As a result, a temperature gradient forms within the cavity, which is crucial for the proper administration of the hydrogel, preventing premature gelation before deposition. Initially, the cavity is at 37ºC, and the areas near the aperture begin to cool as they come into contact with the operating room temperature (20ºC) until reaching a steady state. This phenomenon was also simulated and is illustrated in Fig. 6.

From Fig. 6, it can be observed that it takes between 10 and 15 s to reach a steady state for the air temperature. Therefore, this steady-state temperature profile can be considered as the initial condition for hydrogel injection into the cavity. It is worth noting that the temperature gradient is only present in the first third of the cavity height, where the solution will be injected, and the temperature at the interface is approximately 24ºC, close to room temperature. This detail is crucial to ensure proper administration of the hydrogel, preventing premature gelation before or during injection due to high temperatures at the syringe location.

Considering this temperature profile, the multi-physics model was simulated to study cavity filling coupled with the temperature profile and the evolution of viscosity, as described in Sections 2.3 and 2.4. Fig. 7 illustrates the Volume of Fluid (VOF) for air and the hydrogel solution during the injection process in a 3D view. For enhanced clarity, the cross-sectional view (2D) is depicted in Fig. 8 for the corresponding reported times.

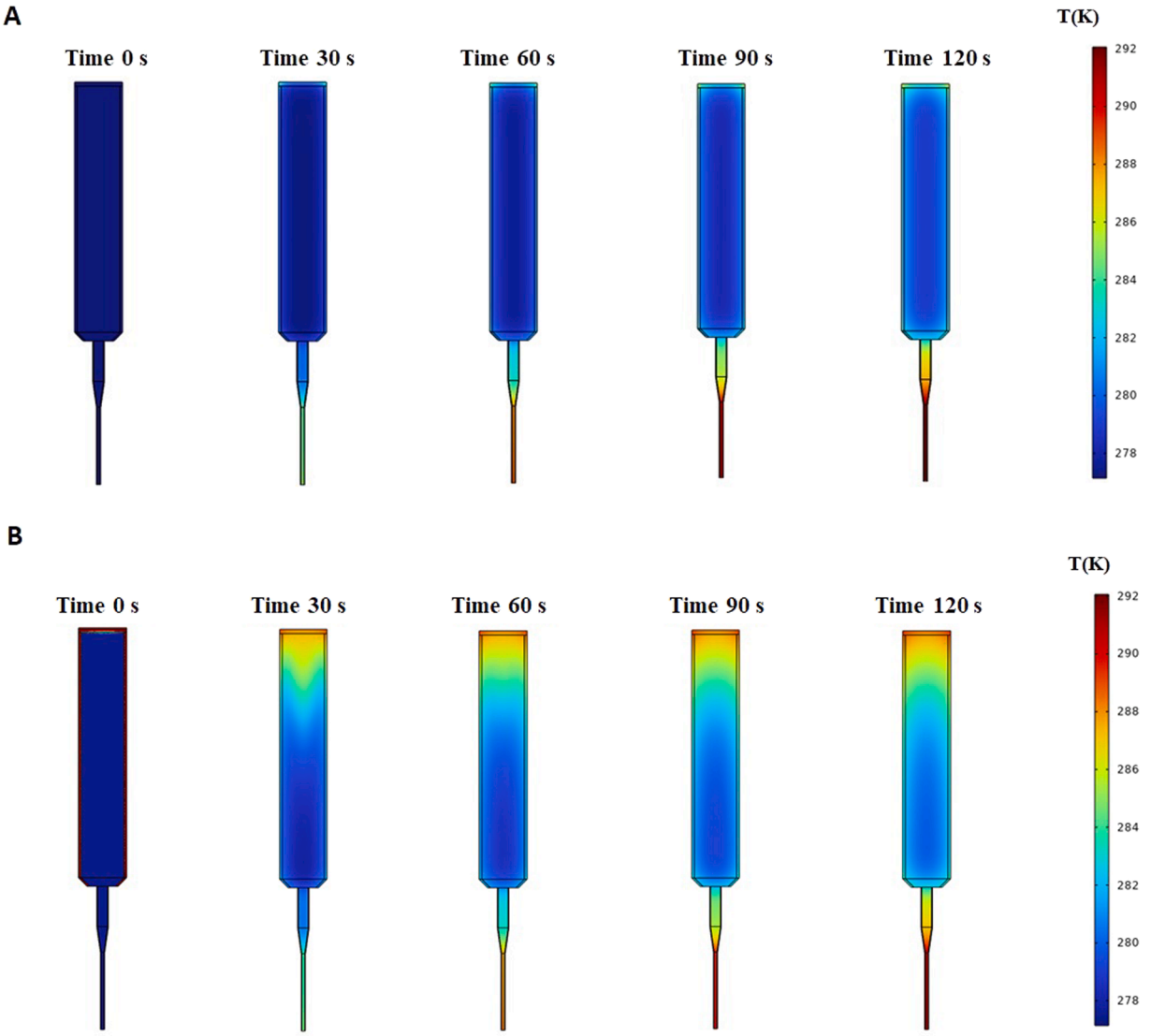

Fig. 5. Temperature plots at different times depending on the syringe and needle storage: A: at 4ºC, B: at 20ºC.

It can be observed that the simulated cavity (12 cm^3 in volume) requires approximately 20 s to be completely filled with the hydrogel solution. The deposition in the cavity appears to be symmetrical when the syringe is positioned at the center of the cavity. In Supplementary material S3, various case studies are presented where the syringe is placed in different positions. From these case studies, it can be concluded that the relative location of the syringe does not significantly affect the filling process, with only a two-second variation in the time required to complete the process across different scenarios. This finding is crucial as the injection in real clinical practice may not always occur precisely in the middle of the cavity.

As per Section 3.2, the administration process should be completed in under 90 s to prevent gelation within the syringe or needle. Based on the findings presented, it can be concluded that there is sufficient time for administration before this phenomenon occurs. This is supported by the fact that after 20 s (the time required for filling), the temperature of the hydrogel in the syringe will be approximately 10ºC (as shown in Fig. 4).

Despite being administered at a temperature below its gelation threshold, the gel undergoes a temperature increase upon deposition into the cavity, triggering the transition phenomenon as described by the kinetics in Equation 15. The temperature distribution within the cavity is influenced by several factors, including the initial temperature of the hydrogel (distinct from the gelation temperature), the temperature at the cavity walls (maintained at 37ºC), and the heat transfer dynamics with the ambient air in the operating room (set at 20ºC). The results of this process are visually represented through a series of cross-sectional images at different time points in Fig. 9.

The results from Fig. 9 demonstrate how the injection alters the temperature distribution in the cavity, with this phenomenon being more pronounced in the initial stages due to the absence of liquid in the cavity. As the cavity fills, the jet profile dissipates, and once the injection ceases, the temperature profile returns to its initial state, influenced solely by the heat transfer process for air until the suture process (see Section 3.4).

Finally, it is important to observe how the viscosity of the hydrogel solution changes due to the heating process, as described by Equation 15. This profile is illustrated in Fig. 10a for a point located in the middle of the cavity. Additionally, for the same location, Fig. 10b shows the VOF parameter (right axis) and the temperature evolution (left axis) over time.

Fig. 10a shows an abrupt increase in viscosity during the first few seconds as air is replaced by the hydrogel solution. Following this, the viscosity increases in a sigmoidal manner, as described by Petkova-Olsson et al. (2018), reaching a maximum value of 9.6 Pa•s after approximately 5 min, according to the experiment detailed in Section

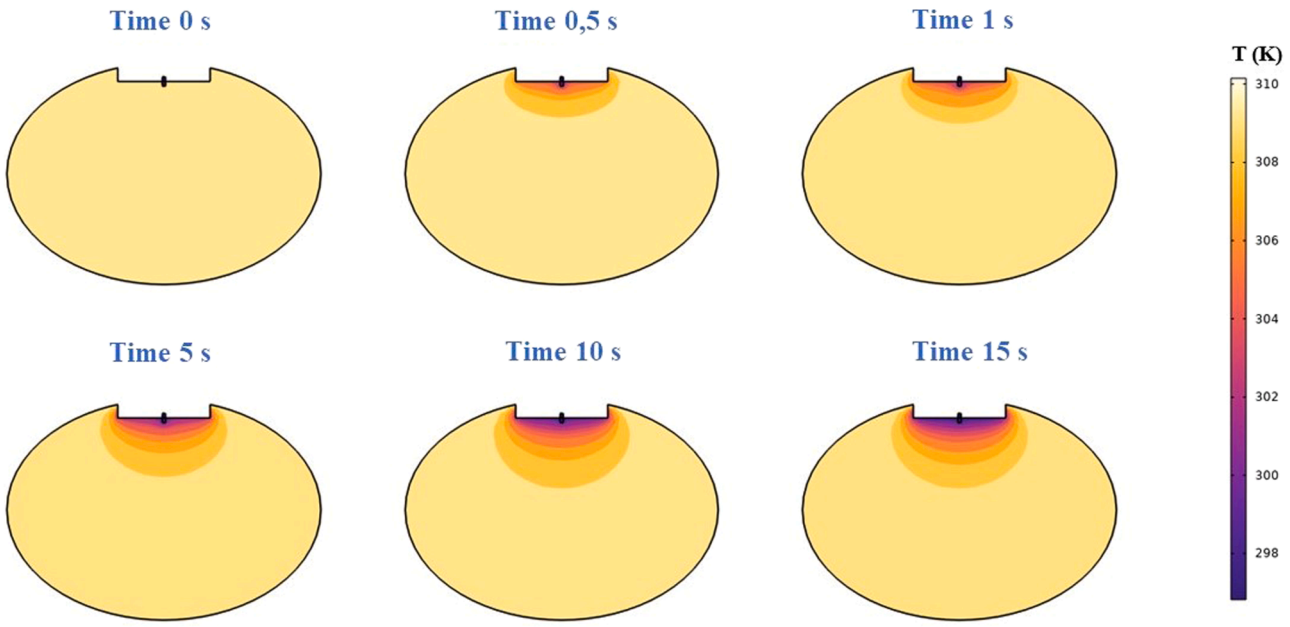

Fig. 6. Temperature evolution in the cavity after resection and before filling with hydrogel (i.e. the cavity filled with air case).

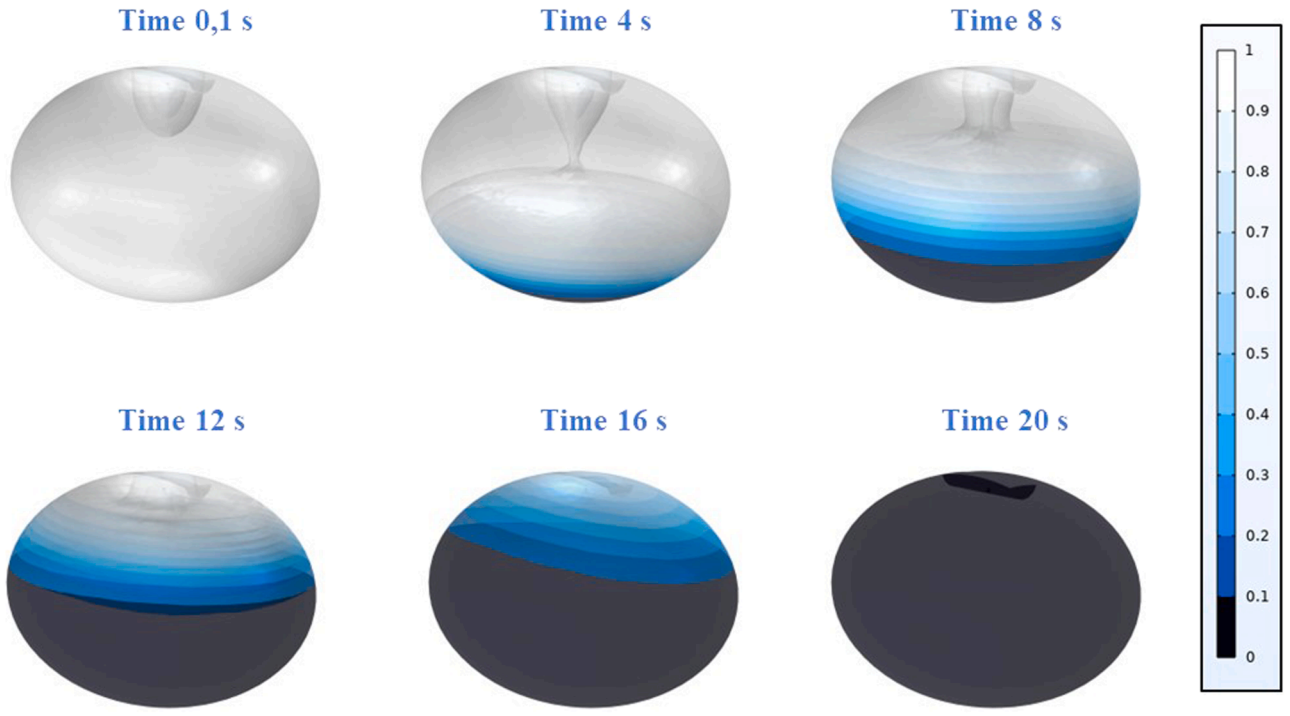

Fig. 7. Time evolution of level set function in 3D. Limits are 0 for hydrogel solution and 1 for air, respectively.

3.1. Consequently, the viscosity remains below 1 Pa•s during the administration process (up to 20 s), ensuring proper distribution within the cavity. At this point, the fluid velocity reaches values around 3 mm s^{-1}.

The profile for VOF represented in Fig. 10b showed small variations during the first five seconds, corresponding to the passage of the jet for that point. After 12 s, the filling was completed at this level (centre of the cavity). The variations in the temperature profile (Fig. 10b) can be explained as follows: Initially, there is a reduction in temperature because the hydrogel is injected at a much lower temperature. Once the filling is complete (around 12 s), the hydrogel temperature increases due to the environmental temperature (37 °C) until approximately 20 s, when the filling process ends for the entire cavity. At this point, there is a plateau indicating a quasi-steady state, controlled by heat transfer with the operating room air. This state is eventually overcome, reaching the final temperature of 309.65 K (36.5ºC). It is notable that 37ºC is not reached because the aperture remains open. This temperature will change during the surgical suture process, as explained in the following section.

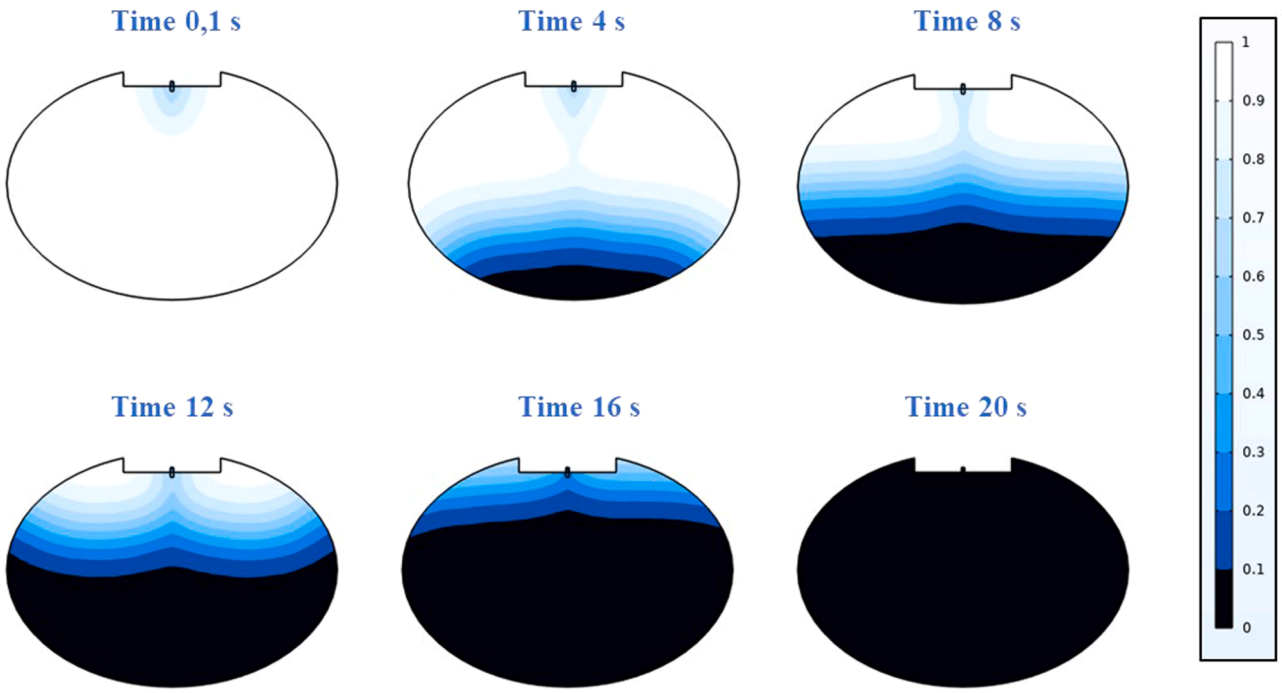

Fig. 8. Same as in the previous figure, only now the level set function contours are shown in the central vertical plane.

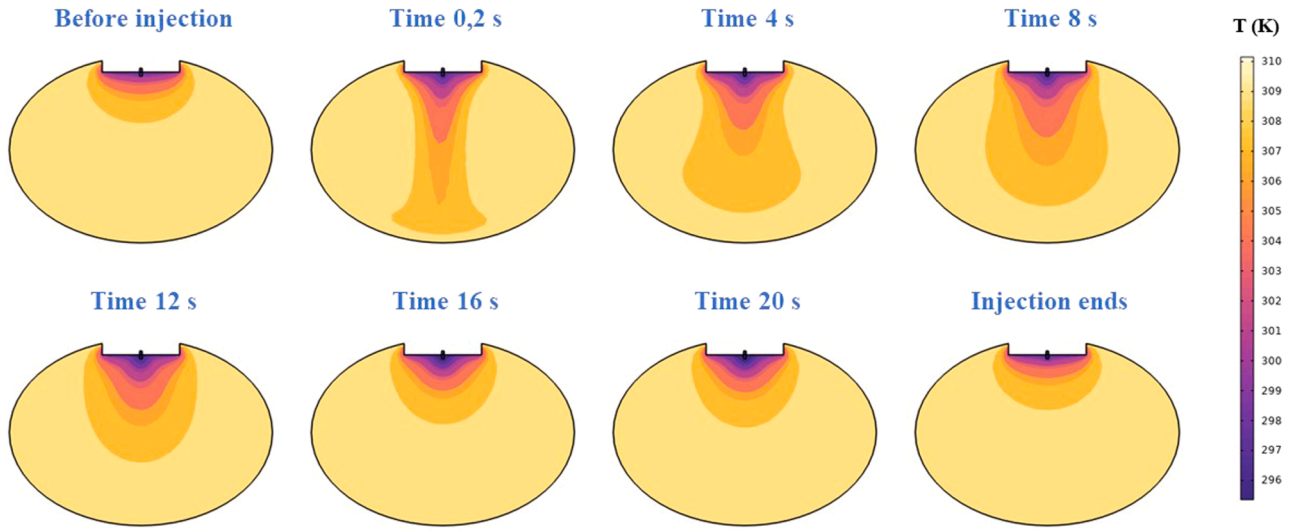

Fig. 9. Temperature contours in the central vertical plane during the cavity filling process.

3.4. After-surgical suture

Once the hydrogel completely fills the cavity, surgeons should sew it. After suturing, there will be no heat transfer to the operation suite. Consequently, the temperature gradient in the cavity will approach zero, resulting in a constant temperature of 37°C throughout. The temperature evolution in the cavity post-sewing was simulated, and the results are shown in Fig. 11.

The results shown in Fig. 11 indicate that it takes 5 min to reach a uniform temperature of 37°C throughout the entire cavity. This occurrence is attributed to the high viscosity of the fluid within the cavity. Upon analyzing the heat flux values at a central point within the cavity, it is evident that the convective heat flux is nearly zero, while the conductive heat flux ranges from 0.1 to 1.5 W/m^2. Hence, conduction emerges as the primary mechanism for heat transfer during the sewing process due to the high viscosity of the fluid. The velocity within the hydrogel is estimated to be approximately 10^{-17} m s^{-1}.

4. Conclusions

A thermosensitive hydrogel, containing poloxamer 407 at various concentrations and Gellan gum, was prepared as a proof of concept for the computational investigation. The hydrogel exhibits a suitable transition temperature, contingent on the poloxamer concentration, along with elastic and viscous modulus values (specifically for the 30 % PF-127 formulation), making it suitable for application as a filling material post-tumor resection surgery.

A multi-physics simulation was carried out to analyze the velocity profile of hydrogel injection alongside temperature variations. The findings revealed that the hydrogel exits the syringe at a velocity of approximately 4 m s^{-1}, requiring 14 s for complete dispensing. The temperature evolution indicates that preserving the hydrogel at 4 °C and

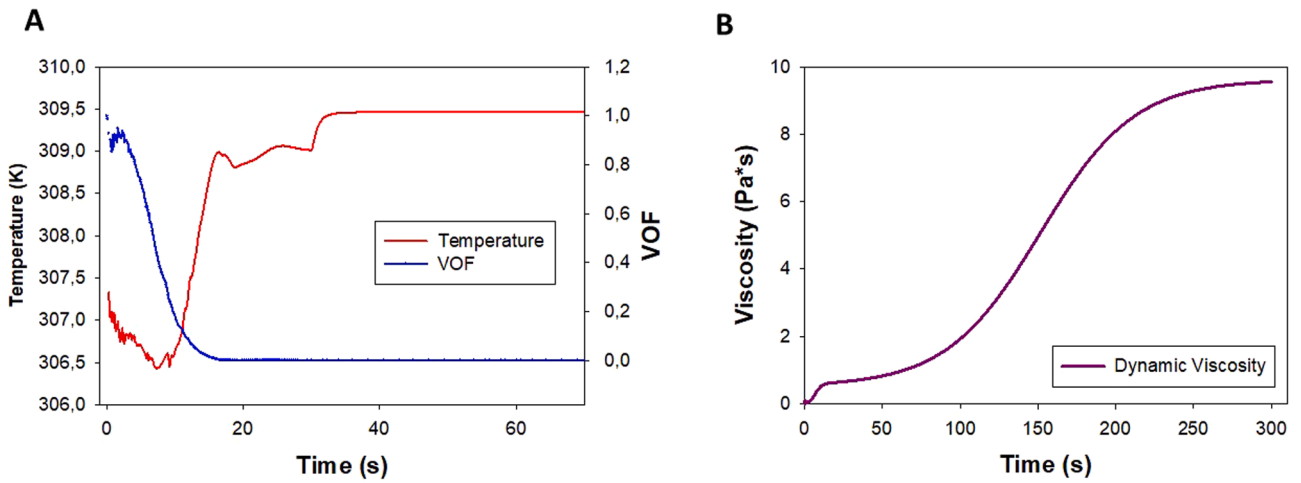

Fig. 10. The time evolution of various parameters at a point located in the center of the cavity includes: (A) hydrogel temperature (left axis), and VOF (right axis); and (B) Viscosity. The Volume of Fluid (VOF) ranges from 1 (air) to 0 (hydrogel) based on the defined initial conditions for the level set-up method.

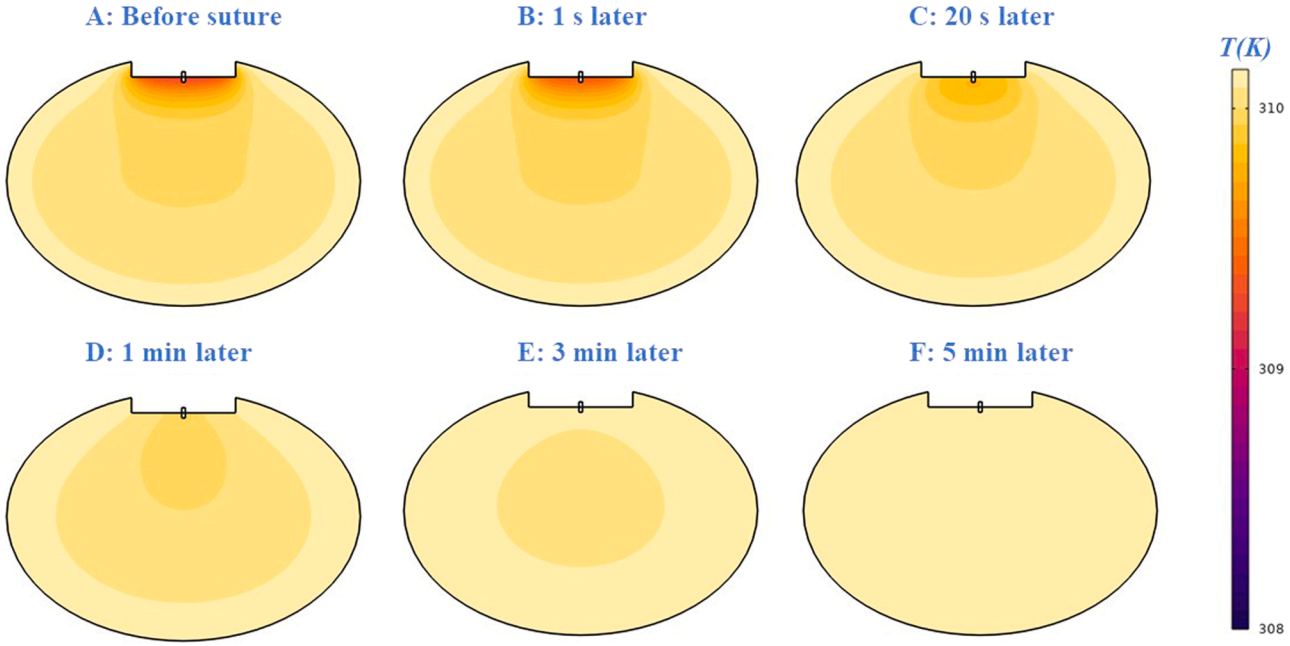

Fig. 11. The time evolution of temperature contours in the cavity filled with hydrogel before and after the sewing process in the central vertical plane.

administering it within 90 s are vital in averting it from attaining the transition temperature of 18 °C.

Moreover, simulations of cavity filling reveal a symmetric distribution of hydrogel disposition, with minimal impact on the filling progress based on the syringe's relative position. Furthermore, the temperature gradient at the cavity's edge appears to impede gelation during the injection process due to the heat exchange with the operating suite. The hydrogel viscosity over time was also modeled, showing a sigmoidal function dependent on temperature and time, requiring five minutes to reach its peak value (9.6 Pa·s). Additionally, the temperature evolution post-suturing was modeled, indicating that only five minutes are necessary to restore a uniform temperature throughout the entire cavity.

In conclusion, this computational study provides support for the potential application of thermosensitive hydrogels in post-tumor surgical treatments. This in silico approximation can be adapted to many different cases, by varying the hydrogel properties, the cavity geometry or the operational conditions. Subsequent research will experimentally validate these models and tailor them to the particular requirements of hydrogel administration in clinical settings.

CRediT authorship contribution statement

Álvaro González-Garcinuño: Writing – original draft, Visualization, Validation, Methodology, Investigation, Formal analysis, Conceptualization. **Antonio Tabernero:** Writing – original draft, Investigation, Formal analysis. **Marcos Blanco-López:** Writing – original draft, Investigation, Data curation. **Eva Martín del Valle:** Writing – review & editing, Supervision, Resources, Project administration. **Sasa Kenjeres:** Writing – review & editing, Validation, Software, Resources, Project administration, Investigation.

Data availability

Data will be made available on request.

Acknowledgements

A. Gonzalez-Garcinuño wants to acknowledge Spanish Ministry of Universities for the research stay grant 'Jose de Castillejo', grant number CAS22/00128. M. Blanco-López wants to acknowledge "Programa propio III de la Universidad de Salamanca: Ayudas para financiar contratos predoctorales de la Universidad de Salamanca cofinanciados por el Banco Santander" for his Phd fellowship. The authors would like to express their gratitude to the Spanish Ministry of Science and Innovation for the financial support, research project: PID2022-1405990B-I00.

Supplementary materials

Supplementary material associated with this article can be found, in the online version, at doi:10.1016/j.ejps.2024.106917.

References

Braet, H., Rahimi-Gorji, M., Debbaut, C., Ghorbaniasl, G., Van Walleghem, T., Cornelis, S., Cosyns, S., Vervaet, C., Willaert, W., Ceelen, W., De Smedt, S.C., Remaut, K., 2021. Exploring high pressure nebulization of Pluronic F127 hydrogels for intraperitoneal drug delivery. Eur. J. Pharm. Biopharm. 169, 134–143.

Bui, T.Q., Cao, V.D., Wang, W., Kjonkisen, A.L., 2021. Recovered energy from salinity gradients utilizing various poly(acrylic acid)-based hydrogels. Polym. (Basel) 13, 645.

Chenite, A., Buschmann, M., Wang, D., Chaput, C., Kandani, N., 2001. Rheological characterisation of thermogelling chitosan/glycerol-phosphate solutions. Carbohydr. Polym. 46, 39–47.

Clegg, J.R., Adebowale, K., Zhao, Z., Mitragotri, S., 2024. Hydrogels in the clinic: an update. Bioeng. Transl. Med. e10680.

Curley, C.J., Dolan, E.B., Cavanagh, B., O'Sullivan, J., Duffy, G.P., Murphy, B.P., 2017. An in vitro investigation to assess procedure parameters for injecting therapeutic hydrogels into the myocardium. J. Biomed. Mater. Res. Part. B. 105, 2618–2629.

De Dios-Pérez, I., González-Garcinuño, A., Tabernero, A., Blanco-López, M., García-Esteban, J.A., Moreno-Rodilla, V., Curto, B., Pérez-Esteban, P., Martin del Valle, E., 2023. Development of a thermosensitive hidrogel base don Polaxamer 407 and gellan gum with inclusion complexes (Sulfobutylated-B-cyclodextrin-farnesol) as a local drug delivery system. Eur. J. Pharm. Sci. 191, 106618.

Desai, P.R., Jain, N.J., Sharma, R.K., Bahadur, P., 2001. Effect of additives on the micellization of PEO/PPO/PEO block copolymer F127 in aqueous solution. Colloid. Surface. A 178, 57–69.

Dewan, M., Sarkar, G., Bhowmik, M., Das, B., Chattoapadhyay, A.K., Rana, D., Chattophadhyay, D., 2017. Effect of gellan gum on the thermogelation property and drug release profile of Poloxamer 407 based ophthalmic formulation. Int. J. Biol. Macromol. 102, 258–265.

Ellis, F.P., 1963. The control of operating-suite temperatures. Brit. J. Industr. Med. 20, 284.

Elstad, N.L., Fowers, K.D., 2009. OncoGel (ReGel/paclitaxel) – Clinical applications for a novel paclitaxel delivery system. Adv. Drug. Deliv. Rev. 61, 785–794.

Emerson, A.E., McCall, A.B., Brady, S.R., Slaby, E.M., Weaver, J.D., 2022. Hydrogel injection molding to generate complex cell encapsulation geometries. ACS. Biomater. Sci. Eng. 8, 4002–4013.

Fan, Y., Ronan, W., Teh, I., Schneider, J.E., Varela, C.E., Whyte, W., McHugh, P., Leen, S., Roche, E., 2019. A comparison of two quasi-static computational models for assessment of intra-myocardial injection as a therapeutic strategy for heart failure. Int. J. Numer. Meth. Biomed. Engng. 35, e3213.

Jons, C.K., Grosskopf, A.K., Baillet, J., Yan, J., Klich, J.H., Saouaf, O.M., Appel, E.A., 2022. Yield-stress and creep control depot formation and persistence of injectable hydrogels following subcutaneous administration. Adv. Funct. Mater. 32, 2203402.

Kok, M., Demirelli, K., Aydogdu, Y., 2008. Thermophysical properties of blend of poly (vinyl chloride) with poly (isobornyl acrylate). Int. J. Sci. Technol. 3, 37–42.

Krisdiyanto, Bin Raja Ghazilla, R.A., Azuddin, M., Bin Ahmad Hairuddin, M.K.F., Risdiana, N., 2023. An analysis of the effect of syringe barrel volume on performance and user perception. Medic. (Baltim.). 102, e33938.

Kushan, E., Senses, E., 2021. Thermoresponsive and injectable composite hydrogels of cellulose nanocrystals and pluronic F127. ACS Appl. Bio. Mater. 4, 3507–3517.

Lacroce, E., Rossi, F., 2022. Polymer-based thermoresponsive hydrogels for controlled drug delivery. Exp. Op. Drug. Deliv. 19, 1203–1215.

Lupu, A., Rosca, I., Gradinaru, V.R., Bercea, M., 2023. Temperature induced gelation and antimicrobial properties of pluronic F127 based systems. Polym. (Basel) 15, 355.

Lv, Q., Yu, S., Quan, F., He, C., Chen, X., 2020. Thermosensitive polypeptide hydrogels co-loaded with two anti-tumor agents to reduce multi-drug resistance and enhance local tumor treatment. Adv. Therap. 3, 1900165.

Mandal, A., Clegg, J.R., Anselmo, A.C., Mitragotri, S., 2020. Hydrogels in the clinic. Bioeng. Transl. Med. 5, e10158.

Marques, A.C., Costa, P.C., Velho, S., Amaral, M.H., 2023. Injectable poloxamer hydrogels for local cancer therapy. Gels. 9, 593.

Meckky, A.B.H., 2020. Computational modelling for specific heat and thermal conductivity of austenitic stainless steel alloys at solid phase. Revue des Composites et des materiaux avances 30, 23–27.

Milocco, A., Scuor, N., Lughi, V., Lamberti, G., Barba, A.A., Divittorio, R., Grassi, G., Perkan, A., Grassi, M., Abrami, M., 2020. Thermal gelation modeling of a pluronic-alginate blend following coronary angioplasty. J. Appl. Polym. Sci. 137, 48539.

Mohammadi, M., Karimi, M., Malaekeh-Nikouei, B., Torkashvand, M., Alibolandi, M., 2022. Hybrid in situ-forming injectable hydrogels for local cancer therapy. Int. J. Pharm. 616, 121534.

Osher, S., Sethian, J.A., 1988. Fronts propagating with curvature-dependent speed: algorithm based on Hamilton-Jacobi formations. J. Comput. Phys. 79, 12.

Petkova-Olsson, Y., Oelschlaeger, C., Ullsten, H., Järnström, L., 2018. Structural, microrheological and kinetic properties of a ternary silica-Pluronic F127-starch thermosensitive system. J. Colloid. Interface. Sci. 514, 459–467.

Phogat, K., Ghosh, S.B., Bandyopadhyay-Ghosh, S., 2023. Recent advances on injectable nanocomposite hydrogels towards bone tissue rehabilitation. J. Appl. Polym. Sci. 140, e53362.

Rossi, S.M., Murray, T.E., Cassidy, J., Lee, M.J., Kelly, H.M., 2019. A custom radiopaque thermoresponsive chemotherapy-loaded hydrogel for intratumoural injection: an in vitro and ex vivo assessment of imaging characteristics and material properties. Cardiovasc. Invervent. Radiol. 42, 289–297.

Saha, Harowicz, M.R., Grimm, L.J., Kim, C.E., Ghate, S.V., Walsh, R., Mazurowski, M.A., 2018. A machine learning approach to radiogenomics of breast cancer: a study of 922 subjects and 529 DCE-MRI features. Br. J. Cancer. 119, 508–516.

Shriky, B., Kelly, A., Isreb, M., Babenko, M., Mahmoudi, N., Rogers, S., Shebanova, O., Snow, T., Gough, T., 2020. Pluronic F127 thermosensitive injectable smart hydrogels for controlled drug delivery system development. J. Coll. Int. Sci. 565, 119–130.

Soni, G., Yadav, K.S., 2014. High encapsulation efficiency of poloxamer-based injectable thermoresponsive hydrogels of etoposide. Pharm. Dev. Technol. 19, 651–661.

Talu, E., Powell, R.L., Longo, M.L., Dayton, P.A., 2008. Needle size and injection rate impact microbubble contrast agent population. Ultrasound. Med. Biol. 34, 1182–1185.

Ul Khaliq, N., Lee, J., Kim, S., Sung, D., Kim, H., 2023. Pluronic F-68 and F-127 based nanomedicines for advancing combination cancer therapy. Pharmaceutics. 15, 2102.

Wang, H., Rodell, C.B., Zhang, X., Dusaj, N.N., Gorman III, J.H., Pilla, J.J., Jackson, B.M., Burdick, J.A., Gorman, R.C., Wenk, J.F., 2018. Effects of hydrogel injection on borderzone contractility post-myocardial infarction. Biomech. Model. Mechanobiol. 17, 1533–1542.

Witika, B.A., Stander, J.C., Smith, V.J., Walker, R.B., 2021. Nano co-crystal embedded stimuli-responsive hydrogels: a potential approach to treat HIV/AIDS. Pharmaceutics 13, 127.

Xanthopoulos, G., Mitropoulos, D., Lambrinos, G., 2012. Estimation of heat and mass transfer coefficients during air-freezing of cucumber. Int. J. Food. Prop. 15, 221–235.

Xu, G., Li, B., Wang, T., Wan, J., Zhang, Y., Huang, J., Shen, Y., 2018. Enhancing the anti-ovarian cancer activity of quercetin using a self-assembling micelle and thermosensitive hydrogel drug delivery system. RSC Adv. 8, 21229–21242.

Yang, X., Gao, L., Wei, Y., Tan, B., Wu, Y., Yi, C., Liao, J., 2021. Phototermal hydrogel platform for prevention of post-surgical tumor recurrence and improving breast reconstruction. J. Nanobiotechnol. 19, 307.

Yu, I., Chen, R., 2021. An experimental and numerical study on coaxial extrusion of a non-Newtonian hydrogel material. J. Manufact. Sci. Eng. 143, 081008.

Yue, P., Feng, J.J., Liu, C., Shen, J., 2004. A diffuse-interface method for simulating two-phase flows of complex fluids. J. Fluid. Mech. 515, 293–317.

Zhang, H., Zhang, M., Zhang, X., Gao, Y., Ma, Y., Chen, H., Wan, J., Li, C., Wang, F., Sun, X., 2022. Enhanced postoperative cancer therapy by ion-based hydrogels. Biomat. Res. 26, 19.